Interpretation of *ab initio* total energy results in a chemical language: II. Stability of $TiAl_3$ and $ScAl_3$

2001 J. Phys.: Condens. Matter 13 11551

(http://iopscience.iop.org/0953-8984/13/50/314)

INSTITUTE OF PHYSICS PUBLISHING JOURNAL OF PHYSICS: CONDENSED MATTER

J. Phys.: Condens. Matter **13** (2001) 11551–11565 PII: S0953-8984(01)28233-2

Interpretation of *ab initio* total energy results in a chemical language: II. Stability of $TiAl_3$ and $ScAl_3$

G Bester and M Fähnle

Max-Planck-Institut für Metallforschung, Heisenbergstrasse 1, D-70569 Stuttgart, Germany

E-mail: faehn@physix.mpi-stuttgart.mpg.de

Received 22 August 2001
Published 30 November 2001
Online at stacks.iop.org/JPhysCM/13/11551

Abstract

The new variant of the energy partitioning scheme introduced in part I of this paper is applied to discuss the relative stabilities of the cubic $L1_2$ structure and the tetragonal $D0_{22}$ structure of $TiAl_3$ and $ScAl_3$ and the stabilization of the $L1_2$ structure of $TiAl_3$ by alloying with divalent transition metal atoms. Furthermore, a striking difference between the covalent bonding energies of $TiAl_3$ and $ScAl_3$ on the one hand and Ni_3Al on the other hand is found.

1. Introduction

The high melting temperature, the good oxidation resistance and the low density of transition-metal (TM) aluminides are attractive properties for high-temperature applications. The lack of ductility at low temperature for some of the aluminum-rich TM compounds has limited their industrial applications. $TiAl_3$ in particular has a very low density ($3.3\ g\,cm^{-3}$) and forms a stable and protecting oxide layer remaining even at high temperatures, but it is very brittle. In the past ten years, many attempts have been undertaken in order to correlate the mechanical properties of TM aluminides with their crystal structure and in a wider scheme with their electronic structure. It was a general belief that the transition from the $D0_{22}$ tetragonal structure to the $L1_2$ cubic structure should ductilize the $TiAl_3$ compound by increasing the number of equivalent $(111)\langle 110\rangle$-type slip systems in order to satisfy the von Mises criterion for slip deformation in polycrystalline samples. The transition from the $D0_{22}$ structure to the $L1_2$ structure in $TiAl_3$ can be achieved by alloying less than 10 at.% late-TM elements [1–7], which substitute for Al in $TiAl_3$ [3, 4, 7]. Despite all these efforts, the resulting $L1_2$ compounds still remain brittle under tensile stress, and the conclusion that $TiAl_3$ is intrinsically brittle can be made.

In this paper we analyse the effect of the tetragonal distortion on the stability of the $D0_{22}$ structure of pure $TiAl_3$ and the stabilization of the cubic $L1_2$ structure upon alloying of $TiAl_3$.

In order to reduce the manifold of observations to the most important features it is advantageous to compare $TiAl_3$ with $ScAl_3$, which is stable in the $L1_2$ structure. With the comparative study of these two materials using the bond indicator E_{cov} introduced in part I of

Table 1. Cut-off radii for the different atom-localized functions.

	Ti	Sc	Al
$r_{\mathrm{s}}^{\mathrm{cut}}$ (au)	5.5	5.5	6.0
$r_{\mathrm{p}}^{\mathrm{cut}}$ (au)	5.5	5.5	6.0
$r_{\mathrm{d}}^{\mathrm{cut}}$ (au)	6.5	6.5	5.5

the paper it is possible to trace back the complex electronic structure of $TiAl_3$ to only a very few striking features. As a last application, a striking difference in the covalent bond energies of $TiAl_3$ and $ScAl_3$ on the one hand and Ni_3Al on the other hand is reported.

2. Application to the structural stability of $TiAl_3$ and $ScAl_3$

2.1. Computational details

The bonding properties were analysed by means of the covalent bond energy E_{cov} introduced in part I of this paper, which requires for its determination data from self-consistent *ab initio* band structure calculations. These calculations were performed within the local-density-functional theory [8–11]. The core–valence interactions were represented by norm-conserving ionic pseudopotentials [12] generated for the atomic configurations Ti($[\mathrm{Ar}]3\mathrm{d}^{2.67}4\mathrm{s}^{0.65}4\mathrm{p}^{0.68}$), Sc($[\mathrm{Ar}]3\mathrm{d}^{1.56}4\mathrm{s}^{0.73}4\mathrm{p}^{0.71}$) and Al($[\mathrm{Ne}]3\mathrm{s}^{2}3\mathrm{p}^{0.7}3\mathrm{p}^{0.3}$). The occupation numbers for Ti and Sc were chosen according to the orbital occupancy obtained from a tight-binding linear-muffin-tin-orbital method [13] calculation for an hcp Ti and Sc crystal at the experimental lattice constant. For Al the pseudopotential used and extensively tested for FeAl, CoAl and NiAl [14–16] has been adopted without any modification. The cut-off radii for the pseudopotential construction were chosen to achieve optimum transferability and fast convergence. The Kohn–Sham effective one-particle equations were solved on a $12 \times 12 \times 12$ Monkhorst–Pack k-point mesh [17] for the tetragonally distorted $D0_{22}$ structures and on a $20 \times 20 \times 20$ Chadi–Cohen [18] k-point mesh for the other structures. The valence electron states were represented by plane waves up to an energy cut-off of 14 Ry and by five localized functions for the Ti and the Sc 3d states. The atom-localized functions for the projection (part I) were optimized with respect to the spillage by varying λ_{vl}, γ_{vl} and r_{vl}^{cut}. The cut-off radii r_{vl}^{cut} were optimized for the $L1_2$ structure in $TiAl_3$ and $ScAl_3$ and kept constant for further calculations. The values adopted for the cut-off radii in all calculations are reported in table 1.

2.2. The stabilizing effect of the tetragonal distortion in $TiAl_3$

The cubic $L1_2$ and the tetragonal $D0_{22}$ structure (figure 1) are closely related. Displacing every second (001) plane of the $L1_2$ structure by a vector $(\frac{1}{2}, \frac{1}{2}, 0)$, which is equivalent to generating a periodic arrangement of anti-phase boundaries, leads to the unrelaxed (i.e. cubic) $D0_{22}$ structure. The nearest-neighbour (NN) environments of the $L1_2$ and of the unrelaxed $D0_{22}$ structures are identical. The Al atoms have eight Al and four TM NN atoms while the TM atoms have 12 Al atoms as NNs. The next-nearest-neighbour (2NN) environments are different for the two structures and were summarized by Hong *et al* [19] in the fact that the $D0_{22}$ structure accommodates more TM–Al 2NN bonds than the $L1_2$ structure. It is important to note that Al has to be classified in two different classes in the $D0_{22}$ structure. The two nonequivalent Al atoms are distinguished in figure 1 by black and grey dots, and the two different kinds of TM–Al bond in the $D0_{22}$ structure, namely the in-plane and the out-of-plane bonds, are referred to as C and D, respectively. Relaxing the c/a-ratio leads from the cubic to the tetragonal $D0_{22}$ structure.

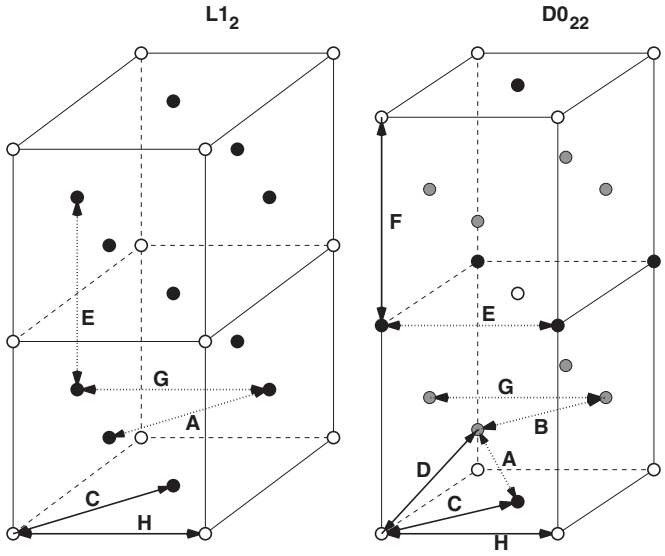

Figure 1. $L1_2$ and $D0_{22}$ structures. Open circles represent TM atoms and the black and grey dots the Al atoms.

We found a lattice constant of 3.91 Å for $TiAl_3$ in the $L1_2$ structure, which is in perfect agreement with the results of previous LMTO calculations [19]. The c/a ratio and the lattice constant of the $D0_{22}$ structure were determined calculating total energies for a set of lattice constants and for ten different c/a ratios. The energy minimum was determined using the fitting procedure according to Rose *et al* [20]. The obtained lattice constant is 3.79 Å with a c/a ratio of 2.23. The experimental values [21] are 3.84 Å for the lattice constant and 2.234 for the c/a ratio, which are close to the calculated values. The tetragonal distortion is found, as in previous publications [19, 22], to be necessary to stabilize the $D0_{22}$ structure. The total energy of the $D0_{22}$ structure with a c/a ratio of 2 (a ratio that we call 'ideal' in the following discussions) lies above the energy of the $L1_2$ structure (figure 2). As a final remark about the structure it should be pointed out that the tetragonal distortion modifies the NN environment since there are two different 'NN' bond lengths. Because this difference is quite small (about 10% for the experimental c/a ratio) and for the sake of simplicity we continue calling the 12 atoms surrounding the Ti or the Al atoms NNs.

To understand the stabilizing effect of the tetragonal distortion on the $D0_{22}$ structure we first calculated the covalent bond energy E_{cov} for the $D0_{22}$ structure for the experimental c/a ratio of 2.234 and for the c/a ratio of 2. Both calculations were performed at the volume of the fully relaxed structure, and they yield very similar results to a calculation at the respective equilibrium volumes of the two structures since both structures have almost the same equilibrium volume (see figure 2). By the distortion of the unit cell at constant volume the atomic density in the (001) plane (in the (100) plane) is increased (decreased). The results for the total covalent bond energy E_{cov}, for the promotion energy E_{prom} and for the sum of both terms $E1$ for the fully relaxed $D0_{22}$ and for the ideal $D0_{22}$ structure are reported in the second and third columns of table 2. In addition, this table shows the gain in total energy due to the structural distortion. The stable structure obtained after the relaxation of the c/a ratio has of course the lowest total energy (by 22.2 mRy) and it has the lowest covalent bond energy by 87 mRy. The promotion energy E_{prom} favours the ideal structure but only by 11 mRy. We therefore clearly see that the

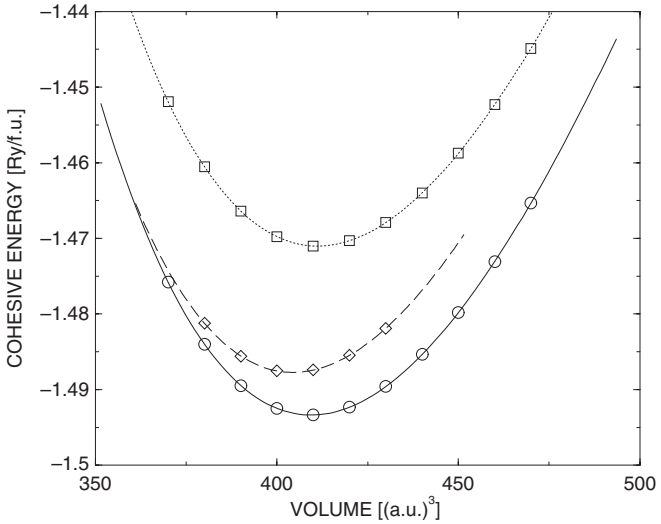

Figure 2. Cohesive energy versus volume for the $L1_2$ structure (dashed curve) and for the tetragonally relaxed ($c/a = 2.234$) (solid curve) and the ideal ($c/a = 2$) $D0_{22}$ structure (dotted curve) of $TiAl_3$.

Table 2. Total covalent bond energy (E_{cov}), promotion energy (E_{prom}) sum, of the total covalent bond energy and the promotion energy $E1$ and total energy differences ΔE_{tot}, all in mRy. Stable structures are marked by a star.

	$TiAl_3$–$L1_2$	$TiAl_3$–$D0_{22}$ ideal	$TiAl_3$–$D0_{22}\star$	$ScAl_3$–$L1_2\star$	$ScAl_3$–$D0_{22}$
E_{cov}	−1609	−1563	−1650	−1607	−1505
E_{prom}	934	921	932	888	872
$E1$	−675	−642	−718	−720	−633
ΔE_{tot}	5.3	22.2	0	0	45.3

stabilization through the relaxation is driven by the covalent part of the total energy. This allows us to draw conclusions about the stabilization effect by looking at this one contribution only.

The results for the dominating bonds are reported in table 3 using the terminology from figure 1 for the different bonds. The most striking features of the bonds in $TiAl_3$ and of the differences between the relaxed and the unrelaxed structures are the following.

(1) The 2NN bonds are without exception much weaker than the NN bonds. The Al–Al and Ti–Al 2NN bonds are antibonding.
(2) The Al–Al and Ti–Al NN bonds have comparable covalent bond energies. The NN Ti–Al bond is not dominating from the point of view of the covalent bond energy, in contrast to an often made assumption in the literature.
(3) The covalent bond energy is less binding in the ideal than in the relaxed structure for all bonds except for the A- and F-bonds, for which the bond energies of the two structures differ by the small amount of 1 mRy only.
(4) The Ti–Al C-bond is significantly strengthened through the relaxation (−46 to −50 mRy).

In the following we shall focus on the last aspect, which seems to be the key to the understanding of the stabilization through the tetragonal distortion. The interplay of 2NNs will be addressed subsequently.

Table 3. Covalent bond energy in mRy for the NN (four left-hand columns) and the 2NN bonds (four right-hand columns) in $TiAl_3$ with relaxed and ideal c/a ratio.

	A (Al–Al)	B (Al–Al)	C (Ti–Al)	D (Ti–Al)	E (Al–Al)	F (Ti–Al)	G (Al–Al)	H (Ti–Ti)
c/a relaxed	−31	−45	−50	−39	−1	+6	+5	−15
c/a ideal	−32	−43	−46	−38	+3	+5	+5	−13

Table 4. Orbital-resolved covalent bond energy for bond C in $TiAl_3$ with a relaxed c/a ratio.

Ti_s–Al_s	Ti_s–Al_p	Ti_s–Al_d	Ti_p–Al_s	Ti_p–Al_p	Ti_p–Al_d	Ti_d–Al_s	Ti_d–Al_p	Ti_d–Al_d
−1.1	−3.8	−0.2	−3.3	−2.1	−0.8	−11.8	−22.2	−4.8

The distance between the Ti and the Al atom along the C-bond is shortened when relaxing the c/a ratio, and the covalent bond energy is increased. This trend, though, cannot be generalized since the NN Ti–Al D-bond, for example, is stronger in the relaxed structure despite the fact that the bond length is increased. The analysis of the results for the orbital- and energy-resolved E_{cov} yields two complementary conclusions.

- The only NN bond which changes significantly when relaxing the structure is the in-plane Ti–Al bond (bond C). All other NN bonds seem to be almost unaffected by the structural relaxation; i.e. the energy- and orbital-resolved E_{cov}-plots are very similar in every respect. The bond energy of every orbital contribution (s–s, s–p, ...) and the shape of every one of the energy-resolved contributions are very similar in the relaxed and in the unrelaxed structures. In other words, the magnitude and shape of the bonding and antibonding peaks in the plots are similar, which yields similar covalent bond strength values.
- The Ti_d–Al_s and the Ti_d–Al_p bonds are the major contributions to the Ti–Al NN bonds (C and D). The orbital-resolved covalent bond energies for the C-bond in the relaxed $TiAl_3$ structure are given in table 4. The Ti_d–Al_p bond is almost twice as strong as the Ti_d–Al_s bond, and all other contributions are significantly weaker.

In figure 3 the energy-resolved covalent bond energy for the Ti_d–Al_p in-plane bond (C) and for the out-of-plane bond (D) are depicted. The difference between the relaxed and the ideal structures for the out-of-plane bond (D) is small. The bond-length of this bond increases when the structure is relaxed but the covalent bond energy does not change significantly. For the in-plane bond (C) the shape of the E_{cov}-curves changes more drastically when the structure is relaxed. The Al_p and Ti_d orbitals hybridize better when the distance between Al and Ti is reduced. The Ti–Al NN bonds, which are dominated by the Ti_d–Al_p contributions, are strengthened when the structure is relaxed, and thus the tetragonally distorted $D0_{22}$ structure is stabilized.

The Al–Al and the Al–Ti 2NN bonds are (table 3) weakly antibonding or non-bonding (for the Al–Al E-bond in the relaxed structure), a behaviour which is unexpected at first, since the NN Al–Al and Al–Ti bonds are strongly bonding and the difference in the distance between the NN and the 2NN is only about 30%. The bond energy strongly depends on the separation of the atoms as well as on the local environment. As an illustrative example for the energy-resolved bond energy between 2NN atoms, the left-hand panel of figure 4 depicts the Ti_d–Al_s 2NN F-bond in the relaxed (thick curves) and the ideal structure (thin curves). The Ti_d–Al_s contribution to the F-bond favours the relaxed structure. The other contributions, for example Ti_d–Al_p shown on the right-hand panel of figure 4, favour the ideal structure, which results in a slightly smaller total covalent bond energy for the relaxed structure. This is shown here to demonstrate the complexity of the bonding process and to caution against

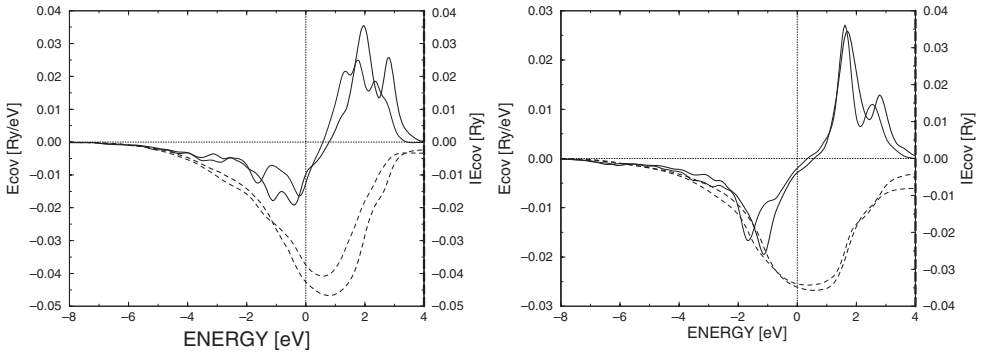

Figure 3. E_{cov}-plot for the $\mathrm{Ti_d}$–$\mathrm{Al_p}$ C-bond (left-hand panel) and D-bond (right panel). The thick (thin) curves are for the relaxed (ideal) structure. Dashed curves are the corresponding integrated quantities. The Fermi energy is set to zero.

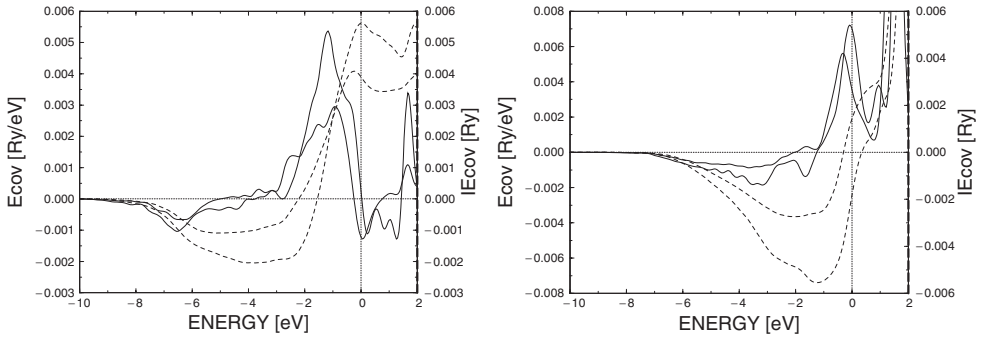

Figure 4. E_{cov}-plot for the $\mathrm{Ti_d}$–$\mathrm{Al_s}$ (left-hand panel) and $\mathrm{Ti_d}$–$\mathrm{Al_p}$ (right-hand panel) 2NN F-bond. The thick (thin) curves are for the relaxed (ideal) structures. Dashed curves are the corresponding integrated quantities. The Fermi energy is set to zero.

jumping to conclusions. The molecular view, in which bonding states and antibonding states are well separated and are filled one after another, is not applicable for the delocalized and very dispersive $\mathrm{Al_s}$ electrons.

The Ti–Ti 2NN bonds are different from the 2NN bonds just discussed. They form strong bonds (table 3), a behaviour that is related to the long range of the d orbitals of Ti, which can overcome the 2NN separation.

To complete the picture of the effect of the relaxation of the c/a ratio on the electronic structure, it is informative to look at the valence electronic density and to notice the changes when the structure is relaxed. Figures 5 and 6 depict the difference between the valence charge densities in the crystal and the superposition of the corresponding atomic charge densities. Regions of charge depletion have dashed contour lines and regions where charge is gained with respect to the superposition of atomic charge densities are marked by solid contour lines. Figure 5 displays the (001) plane with a mixed atomic composition, and figure 6 shows the (010) plane. The contour lines are separated by 0.001 electrons au^{-3} for all the plots. The C-bond and the D-bond are in the depicted planes between the Ti and the Al atoms.

These plots support the general belief that when the interaction between the atoms is switched on and the electrons are allowed to hybridize the valence electron density in the region between the atoms is increased while it is decreased at the atom positions. This increase in the electron valence charge density in the interstitial region in visible in all the plots.

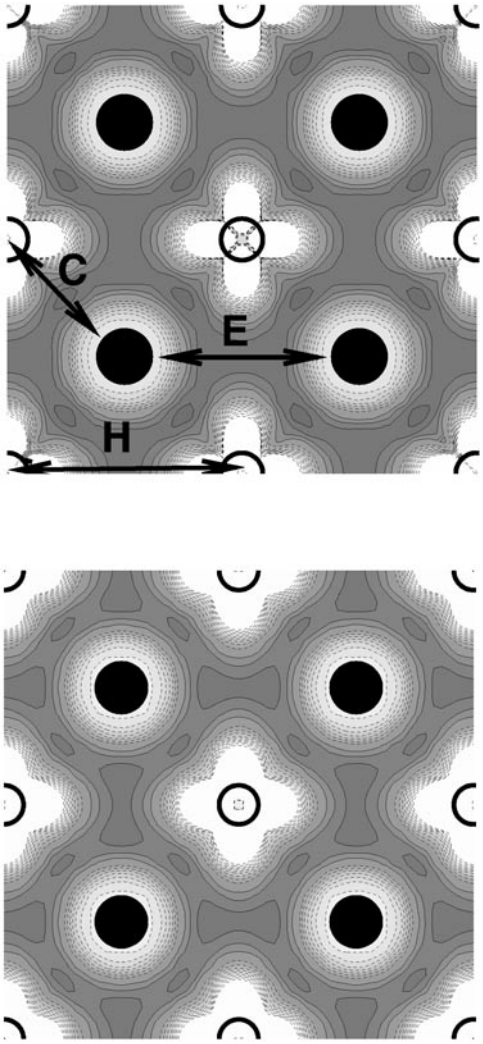

Figure 5. Difference between the valence charge density in the $D0_{22}$ crystal and the superposition of the corresponding atomic charge densities in the (001) plane. The c/a ratio is relaxed in the upper panel and ideal in the lower panel. The Ti (Al) atoms are marked by open (filled) circles.

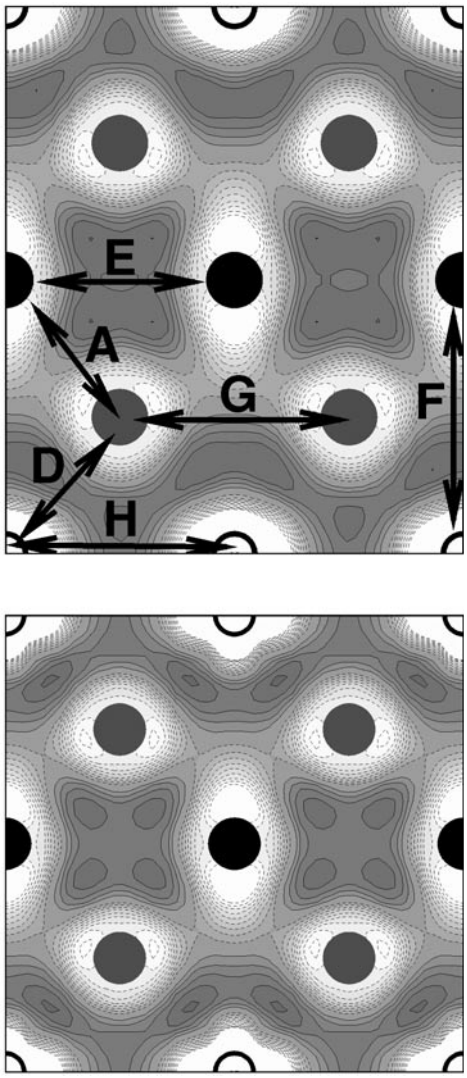

Figure 6. Difference between the valence charge density in the $D0_{22}$ crystal and the superposition of the corresponding atomic charge densities in the (010) plane. The c/a ratio is relaxed in the upper panel and ideal in the lower panel. The Ti (Al) atoms are marked by open (filled) circles.

The striking difference between the plots for the relaxed and the plots for the ideal structure is that the absolute value of the charge differences, negative as well as positive, are overall larger in the relaxed structure. The regions of charge depletion lack more electrons in the relaxed structure than in the ideal structure and the regions of increased valence electron densities contain more electrons in the relaxed structure than in the ideal structure. The difference charge densities along the C-, the H- and the E-bond (all of which are in the plane depicted in figure 5) are larger in the relaxed than in the ideal structure. This observation is compatible with the idea that stronger covalent bonds have higher interatomic electron densities. However, this general

Table 5. Covalent bond energy in mRy sorted by bonds (see figure 1 for the terminology of the bonds) for $TiAl_3$ and $ScAl_3$ in the $L1_2$ and in the $D0_{22}$ structure. Stable structures are marked by a star.

	A (Al–Al)	B (Al–Al)	C (TM–Al)	D (TM–Al)	E (Al–Al)	F (TM–Al)	G (Al–Al)	H (TM–TM)
$TiAl_3$ $D0_{22}\star$	−31	−45	−50	−39	−1	+6	+5	−15
$ScAl_3$ $D0_{22}$	−34	−43	−39	−33	+2	+4	+6	−12
$TiAl_3$ $L1_2$	−38		−40		+4		+11	−9
$ScAl_3$ $L1_2\star$	−39		−37		+3		+12	−9

Table 6. Bond order sorted by bonds (see figure 1 for the terminology of the bonds) for $TiAl_3$ and $ScAl_3$ in the $L1_2$ and in the $D0_{22}$ structure. Stable structures are marked by a star.

	A (Al–Al)	B (Al–Al)	C (TM–Al)	D (TM–Al)	E (Al–Al)	F (TM–Al)	G (Al–Al)	H (TM–TM)
$TiAl_3$ $D0_{22}\star$	0.078	0.136	0.141	0.110	0.000	−0.004	−0.005	0.020
$ScAl_3$ $D0_{22}$	0.092	0.117	0.111	0.099	−0.002	−0.003	−0.005	0.014
$TiAl_3$ $L1_2$	0.105		0.112		−0.004		−0.009	0.011
$ScAl_3$ $L1_2\star$	0.104		0.108		−0.003		−0.009	0.011

assumption has to be made with care since the 2NN Ti–Al F-bond is weaker in the relaxed structure despite the fact that the valence charge density between these two atoms is larger in the relaxed than in the ideal structure as shown in figure 6. The same kind of observation is made for the Ti–Al NN bond D, which is stronger in the relaxed structure with a lower interatomic valence charge density. Relaxing the structure makes the Ti atoms more isotropic in the (010) plane and less isotropic in the (001) plane while the Al atoms seem to be mostly unaffected by the structural relaxation.

2.3. The competition between the $L1_2$ and $D0_{22}$ structure

To study the structural stability of $TiAl_3$, it is interesting to compare it with a TM aluminide that crystallizes in the competing $L1_2$ structure. The best candidate is probably $ScAl_3$ since it has one electron less than $TiAl_3$ and is stable in the $L1_2$ structure. To compare the two materials we performed a detailed analysis of E_{cov} and the bond order; the results are reported in tables 5, 6 and 2. The calculations for $ScAl_3$ in the $D0_{22}$ structure were performed at the fully relaxed c/a ratio of 2.16 and at the LDA lattice constant of 3.944 Å as well as for the ideal c/a ratio of 2 at the same volume as the relaxed structure. The results reported are for the fully relaxed structure but the differences between the two different approaches are small and the conclusions drawn do not dependent on the procedure used.

In the first place we notice that the total bond energy, E_{cov}, in table 2 is larger for the stable structure in $TiAl_3$ as well as in $ScAl_3$. Thus, the gain in the covalent bond energy when going from the unstable to the stable structure has the same sign as the gain in total energy, but it is larger (see table 2). Again, this clearly demonstrates that the process of structural stabilization is driven by the covalent bond energy. The promotion energy seems to be almost insensitive to the structural changes between the $L1_2$ and the $D0_{22}$ structure and will not be addressed in the following discussion.

In a further step of refinement it is instructive to analyse the results bond by bond, as reported in table 5. The Al–Al NN bonds are quite similar in both materials, but major differences appear in the TM–Al bonds. In the following we shall compare the covalent bond energy of the NN TM–Al bond in the $L1_2$ structure (bond C) with the bond energy of the

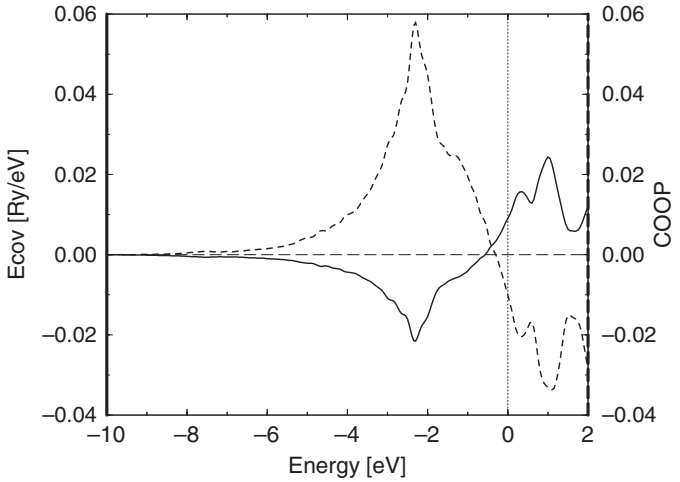

Figure 7. Covalent bond energy (solid curve) and crystal orbital overlap population COOP (dashed curve) for the Ti_d–Al_p bond in the $L1_2$ structure. The Fermi energy is set to zero.

corresponding bonds C and D of the $D0_{22}$ structure. The comparison yields two qualitatively different conclusions for $ScAl_3$ and $TiAl_3$. In $ScAl_3$ the covalent bond energy of bond C is similar in both structures while the out-of-plane bond D of the $D0_{22}$ structure is weaker than bond C of the $L1_2$ structure. In $TiAl_3$ the covalent bond energy of bond D in the $D0_{22}$ structure is almost identical with that of bond C in the $L1_2$ structure. The in-plane bond C of the $D0_{22}$ structure is stronger than bond C of the $L1_2$ structure. In a simplified formulation, the splitting of bond C of the $L1_2$ structure into bonds C and D of the $D0_{22}$ structure is different for the two materials; it strengthens bond C in $TiAl_3$ and weakens bond D in $ScAl_3$.

In table 6 the values of the bond order (see section 2 of part I) are given in the same manner as done for the covalent bond energy in table 5. Qualitatively, both bonding indicators yield the same information. There are some minor quantitative differences but the trends are the same. In figure 7 the energy-resolved bond order, i.e. the crystal orbital overlap population (COOP), and the corresponding covalent bond energy are plotted for the NN-Ti_d–Al_p bond in the $L1_2$ structure. Qualitatively the two curves are very similar. The information about the ratio between the strength of bonding to antibonding peaks is different, though. The analysis of the covalent bond energy attributes a similar strength to both peaks while the COOP analysis predicts a stronger bonding contribution. Nevertheless, the information obtained from the charge partitioning analysis is, for at least a qualitative or a semi-quantitative analysis of this system, valuable. Since the computational effort for the COOP analysis is much smaller than for the covalent bond energy method, charge partitioning remains a very attractive tool for any qualitative bond analysis, at least for this Ti–Al compound.

It is possible with the use of the energy-resolved E_{cov} to analyse the above-discussed results in a detailed manner. The energy-resolved E_{cov}-plots and the corresponding integrated quantities $I\,E_{cov}$ are depicted in figure 8 for $ScAl_3$ and in figure 9 for $TiAl_3$. From the various orbital contributions to the C- and D-bonds we chose to analyse the TM_d–Al_p bond because it is the dominant part (see table 4). All other contributions together play a minor role and will not be addressed in detail.

The value of $I\,E_{cov}$ at the Fermi energy is the bond energy of the TM_d–Al_p bond. In the $L1_2$ structure the Sc_d–Al_p bond (left-hand panel of figure 8) is as strong as it can be. The Fermi level lies exactly between the filled bonding states and the unfilled antibonding states.

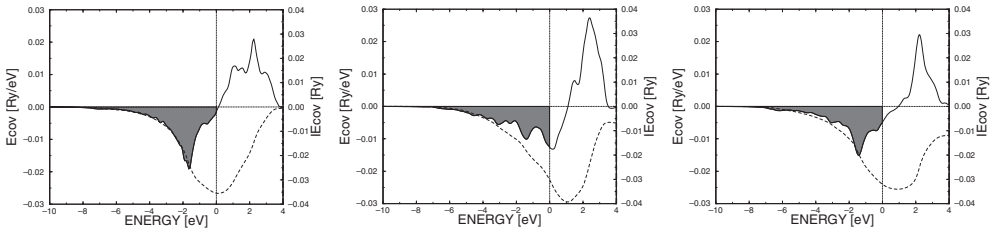

Figure 8. Covalent bond energies E_{cov} (solid curves) and the corresponding integrated quantities IE_{cov} (dashed curves) for $ScAl_3$. The left-hand, middle and right-hand panels depict the Sc_d–Al_p C-bond in the $L1_2$ structure and the in-plane (C-bond) and the out-of-plane (D-bond) Sc_d–Al_p bond in the $D0_{22}$ structure, respectively.

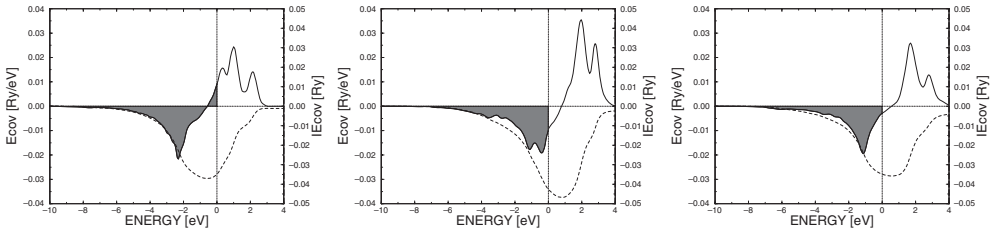

Figure 9. Covalent bond energies E_{cov} (solid curves) and the corresponding integrated quantities IE_{cov} (dashed curves) for $TiAl_3$. The left-hand, middle and right-hand panels depict the Ti_d–Al_p C-bond in the $L1_2$ structure and the in-plane (C-bond) and the out-of-plane (D-bond) Ti_d–Al_p bond in the $D0_{22}$ structure, respectively.

The integrated covalent bond energy has its maximum at the Fermi energy, and any shift in the Fermi level would lower the bond energy of this bond. For $TiAl_3$ in the same structure (left-hand panel of figure 9), the Ti_d–Al_p bond does not fulfill this optimum condition. Antibonding states are starting to become filled at about 0.8 eV below the Fermi level, and this lowers the covalent bond energy of the bond and destabilizes the structure. The situation for the same material in the $D0_{22}$ structure is quite different. The states filled in the two NN Ti–Al bonds C and D are purely bonding states. There is no weakening of the bonds through the filling of antibonding states as in the $L1_2$ structure. In other words, the structural change from the $L1_2$ to the $D0_{22}$ structure results in a depopulation of antibonding Ti_d–Al_p states, leading to a stabilization of the $D0_{22}$ structure. The situation for $ScAl_3$ is different. The Sc_d–Al_p bonds in the $D0_{22}$ structure are weaker not because antibonding states are filled but because many bonding states remain unoccupied.

The comparison of figure 9 with 8 shows that the rigid-band model is fairly well fulfilled. The covalent bond energy plots and hence the dispersion relations do not seem to change qualitatively but are only shifted on the energy scale. This observation is particularly striking when looking at the occupied Al_s–Al_s bonds in $ScAl_3$ and $TiAl_3$ (figure 10). Applying this model enables us to understand the progressive stabilization of the $D0_{22}$ structure when going from $ScAl_3$ to VAl_3 via $TiAl_3$ [22]. A shift of the Fermi level to the right of the Fermi level of $TiAl_3$, keeping the band structure unchanged, simulates the replacement of Ti by V. By doing so, some antibonding states in the V_d–Al_p bond for the $L1_2$ structure and some bonding states for the $D0_{22}$ structure will be additionally filled. The $L1_2$ structure, which was only slightly less favourable than the $D0_{22}$ structure in $TiAl_3$, is now definitely unfavourable compared with the $D0_{22}$ structure. The in-plane as well as the out-of-plane bonds in $D0_{22}$–VAl_3 will probably be optimum: all bonding states are occupied and all antibonding states are unoccupied. This

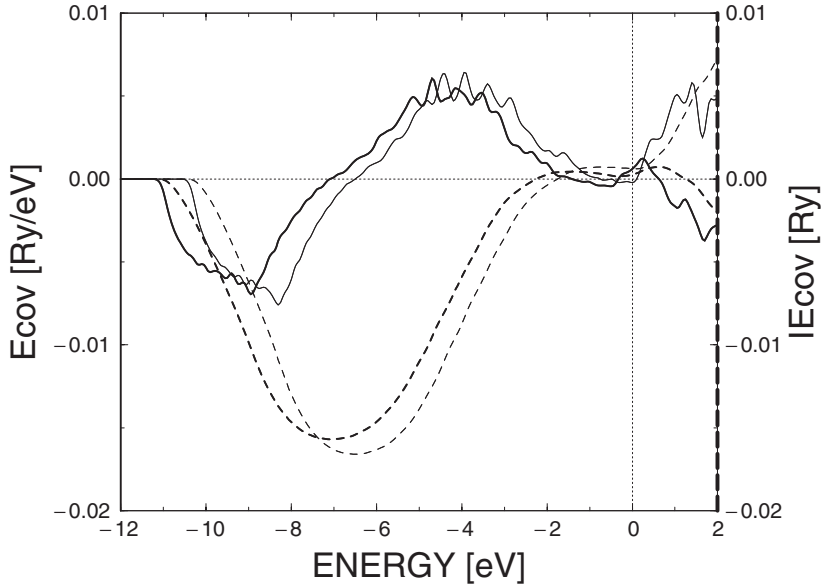

Figure 10. Covalent bond energies E_{cov} (solid curves) and the corresponding integrated quantities IE_{cov} (dashed curves) for $TiAl_3$ (thick curves) and for $ScAl_3$ (thin curves) for the Al_s–Al_s bond in the $L1_2$ structure.

view within the rigid-band model is confirmed by calculations of Carlsson and Meschter [22], that showed VAl_3 to be lower in energy in the $D0_{22}$ structure, even without relaxing the c/a ratio. The atomic-size effect, that could play an important role in this discussion and which would be described by the pair-potential term in the energy-partitioning scheme, seems to be not necessary to obtain the right trends.

For $CrAl_3$ or $MnAl_3$ and for the late TM aluminides, antibonding states will start to become filled in the TM_d–Al_p bonds of the $D0_{22}$ structure, and therefore other structures, not presented here, will be more favourable.

Another classical application of the rigid-band model is the simulation of doping by a shift of the Fermi energy. $TiAl_3$ is a perfect example for such an approach. By alloying divalent TM atoms that will replace the trivalent Al atoms in $TiAl_3$ the antibonding Ti_d–Al_p states of the $L1_2$ structure will be depopulated. By the same procedure, bonding states of the $D0_{22}$ structure are depopulated, resulting in a stabilization of the $L1_2$ structure and a destabilization of the $D0_{22}$ structure. In this particular case of $TiAl_3$ the explanation using electronic structure arguments is particularly simple, and the well known experimental stabilization of the $L1_2$ structure through alloying [1–7] with late TM elements can be traced back to the Ti_d–Al_p bond.

One method for the interpretation of electronic structure data is to use the Mulliken electron partitioning approach. It is sometimes used to get a grasp on the bonding (with the introduction of the COOPs as explained in section 2 of part I) and particularly to have an idea about the ionicity when the values of the Mulliken charges at the various atoms are compared. There are two different approaches to partition the charge in a compound using the means of electronic structure calculations for extended systems. The first one is to integrate the charge located within a certain sphere around each atom. This method emphasizes the electrostatic point of view, but the so-defined quantity depends on the chosen radii of integration. In such an approach, some of the charge is not attributed to any atom or is attributed twice when the spheres

Table 7. Mulliken's population analysis, $q_{i\alpha} - N_{i\alpha}^{\text{free atom}}$, for $TiAl_3$ and $ScAl_3$ in the $L1_2$ and in the $D0_{22}$ structure. There are two crystallographically different Al atoms in the $D0_{22}$ structure and the results for them are given in two different lines.

	Al_{tot}	Al_s	Al_p	Al_d	TM_{tot}	TM_s	TM_p	TM_d
$TiAl_3$ $L1_2$	0.038	−0.759	0.744	0.053	−0.115	−1.569	0.248	1.206
$TiAl_3$ $D0_{22}$	−0.060	−0.697	0.584	0.055	−0.055	−1.553	0.357	1.140
	0.058	−0.768	0.778	0.048				
$ScAl_3$ $L1_2$	0.094	−0.705	0.756	0.042	−0.281	−1.687	0.243	1.166
$ScAl_3$ $D0_{22}$	0.007	−0.654	0.615	0.047	−0.332	−1.619	0.273	1.014
	0.162	−0.678	0.806	0.036				

are chosen to overlap. The second approach, adopted here, is Mulliken's analysis in terms of occupation of orbitals localized at the various atoms. This procedure emphasizes the covalent character of the material. The results for the differences $q_{i\alpha} - N_{i\alpha}^{\text{free atom}}$ in $TiAl_3$ and in $ScAl_3$ are reported in table 7. The configurations $N_{i\alpha}^{\text{free atom}}$ were $3s^2 3p^1$ for Al, $3d^2 4s^2 4p^0$ for Ti and $3d^1 4s^2 4p^0$ for Sc. The values for the total charge differences located on each atom are about zero, which means that the total charge located on each atom is about equal to the total atomic charge. For $ScAl_3$ we report some charge 'transfer' (by transfer we mean transfer between orbitals as already pointed out) to the Al atoms, which gain about 0.1 electron/atom from the Sc atoms; in $TiAl_3$ there is a smaller charge transfer. (This observation is in contradiction to that made for the B2 late TM aluminides FeAl, CoAl and NiAl, where a charge transfer of about one electron from Al to the TM atoms was found with Mulliken's analysis [23] as well as with the atomic-sphere integration method [24].) The charge redistribution within the atoms, i.e. the promotion, is very similar in both compounds and in both structures. In Al there is a donation of about 0.7 electrons from the s channel to the p channel. The crystallographically different Al atoms have a slightly different population of the p channel. The results for the shaded Al atoms in figure 1 are given in the second row in table 7. These atoms have about 0.2 electrons more in the p channel than the solid Al atoms in figure 1 (third row in table 7). This is an effect of the different 2NN environments of these atoms. The shaded atoms have six 2NN Al atoms while the solid atoms have four 2NN Al and two 2NN TM atoms. The Al d channel is only weakly populated. In Ti and Sc the s electrons are promoted to the p and mainly to the d channel. Again, no striking differences are observed comparing Mulliken's charges at the TM site in $TiAl_3$ and $ScAl_3$. A general conclusion for the analysis of Mulliken's charge is that the early TM trialuminides are redistributing their charge within the individual atoms, whereas the late TM aluminides in the B2 structure are transferring charge from the Al orbitals to the TM orbitals.

In order to complete the investigation we plotted the difference valence charge densities for the two compounds in the $D0_{22}$ structure for the (010) plane in figure 11. The centre parts of the two plots where the NN Al–Al bonds are visible are almost identical in both compounds. The difference charge densities at the aluminum atoms and between the Al atoms are mostly unchanged when Ti is exchanged by Sc. This observation follows the tendency in the E_{cov}-analysis: the covalent bond energies of the NN Al–Al bonds (table 5) are very similar in the two compounds. The difference charge density along the H TM–TM bond is also very similar in the two compounds, and the covalent bond energy of the H-bond is quite similar, with −15 mRy in $TiAl_3$ and −12 mRy in $ScAl_3$. There is a striking accumulation of charge between the 2NN Ti and Al atoms along bond F that is almost completely missing from $ScAl_3$. Against the common interpretation, this feature is not correlated with an increase of the covalent bond

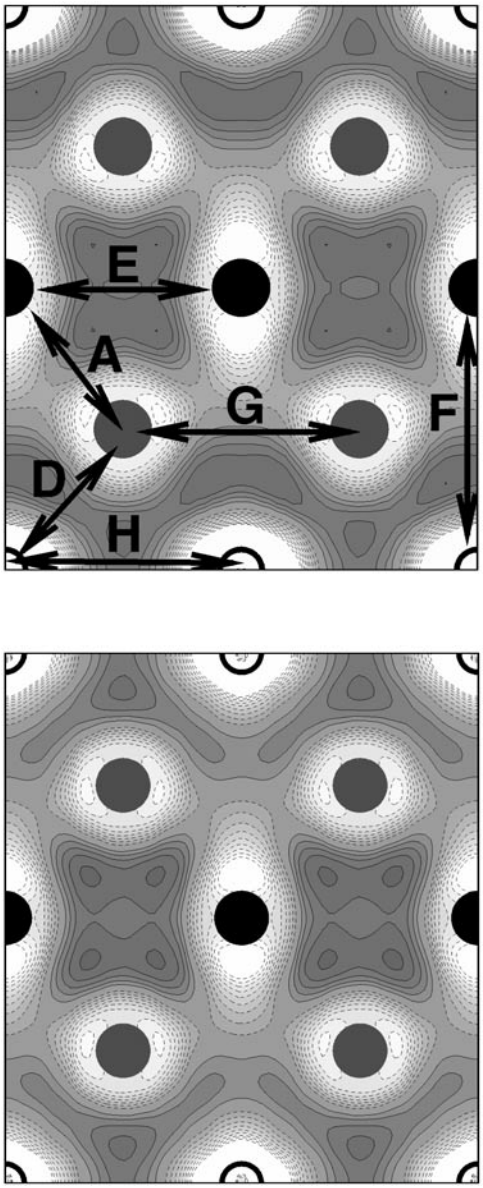

Figure 11. Difference between the valence charge density in the $D0_{22}$ crystal and the superposition of the corresponding atomic charge densities in the (010) plane for relaxed $TiAl_3$ (upper panel) and relaxed $ScAl_3$ (lower panel). The Ti (Al) atoms are marked by open (filled) circles.

energy, since the 2NN TM–Al F-bond is weaker in $TiAl_3$ than in $ScAl_3$. This same pile-up of charge is presumably filling bonding NN Ti–Al states of bond D, which would explain the greater covalent bond energy in $TiAl_3$ (39 mRy) compared with that of $ScAl_3$(33 mRy).

Finally, we remark a striking difference between $TiAl_3$ and $ScAl_3$ on the one hand and Ni_3Al on the other hand for the behaviour of the covalent bond energies when going from the $L1_2$ structure to the $D0_{22}$ structure. The TM–Al bond in the $L1_2$ structure (C) splits in the $D0_{22}$ structure into the bonds C and D. In $TiAl_3$ this splitting results in two very different bonds (see table 5). The C-bond of the $L1_2$ structure corresponds to a bond energy of -40 mRy and the C- and D-bonds of the $D0_{22}$ structure to -50 and -39 mRy, respectively. This observation holds for the Al–Al bonds as well. The A-bond with a bond energy of -38 mRy in the $L1_2$

structure splits into bonds A and B in the $D0_{22}$ structure with the bond energies −31 and −45 mRy. The situation is completely different in Ni_3Al as depicted in table 8. The C-bond in the $L1_2$ structure with a bond strength of −50 mRy splits into two bonds with very similar bond energies, namely −49 mRy for bond C and −50 mRy for bond D. The A bond in the $L1_2$ structure with a bond energy of −30 mRy splits into bond A with −29 mRy and bond B with −28 mRy. The change of the 2NN environment when going from the $L1_2$ to the $D0_{22}$ structure has almost no effect on the NN bond energy in Ni_3Al but a tremendous effect in $TiAl_3$ or in $ScAl_3$. This difference has something to do with the degree of directionality of the bonds and is therefore possibly related in some way to the ductility of Ni_3Al and the brittleness of $TiAl_3$.

Table 8. Covalent bond energy in mRy for the NN (four left-hand columns) and the 2NN bonds (four right-hand columns) in Ni_3Al with $L1_2$ and $D0_{22}$ structure. See figure 1 for the terminology of the bonds.

	A (Ni–Ni)	B (Ni–Ni)	C (Al–Ni)	D (Al–Ni)	E (Ni–Ni)	F (Ni–Al)	G (Ni–Ni)	H (Al–Al)
$L1_2$	−30		−50		+3		+1	−5
$D0_{22}$	−29	−28	−49	−50	+3	−2	+2	−3

The second striking point is that the NN bonds in $TiAl_3$ or in $ScAl_3$, i.e. TM–Al and Al–Al, are of similar strength while the NN Ni–Ni bonds in Ni_3Al are significantly weaker than the NN Ni–Al bonds. This could explain the isotropic elastic constants of $TiAl_3$ and the anisotropic elastic constants of Ni_3Al, but a detailed analysis is required to make definite conclusions.

3. Conclusion

In this paper we have demonstrated the power of the energy-partitioning scheme developed in part I by discussing the relative stabilities of the cubic $L1_2$ structure and the tetragonal $D0_{22}$ structure of $TiAl_3$ and $ScAl_3$. The main results are the following.

(1) For these systems the covalent bond energies for the NN bonds are much larger than those for the further distant bonds.
(2) The stabilization of the $D0_{22}$ structure by the tetragonal distortion is related to a strengthening of a Ti_d–Al_p NN bond.
(3) The stabilization of the $L1_2$ structure of $TiAl_3$ when alloying with divalent TM atoms against the $D0_{22}$ structure of pure $TiAl_3$ can be traced back to the filling of bonding (antibonding) Ti_d–Al_p states for the $L1_2$ ($D0_{22}$) structure.
(4) There are hints at a stronger directionality of the bonds in $TiAl_3$ and $ScAl_3$ as compared with Ni_3Al. Possibly this is related in some way to the ductility of Ni_3Al and the brittleness of $TiAl_3$.

References

[1] Eberhart M E, Kumar K S and MacLaren J M 1990 *Phil. Mag.* B **61** 943
[2] Nic J P, Zhang S and Mikkola D E 1990 *Scr. Metall. Mater.* **24** 1099
[3] Carlsson A E and Meschter P J 1990 *J. Mater. Res.* **5** 2813
[4] Hong T and Freeman A J 1991 *J. Mater. Res.* **6** 330
[5] Prakash U, Buckley R A, Jones H and Sellars C M 1992 *J. Mater. Sci.* **27** 2001
[6] Durlu N and Inal O T 1992 *J. Mater. Sci.* **27** 3225
[7] Liu S Y, Hu R Z and Wang C Y 1994 *Solid State Commun.* **92** 303
[8] Hohenberg P and Kohn W 1964 *Phys. Rev.* **136** B 864

[9] Kohn W and Sham L J 1965 *Phys. Rev.* **140** A 1133
[10] Ceperley D M and Alder B J 1980 *Phys. Rev. Lett.* **45** 566
[11] Perdew J P and Zunger A 1981 *Phys. Rev.* B **23** 5048
[12] Vanderbilt D 1985 *Phys. Rev.* B **32** 8412
[13] Andersen O K and Jepsen O 1984 *Phys. Rev. Lett.* **53** 2571
[14] Fähnle M, Mayer J and Meyer B 1999 *Intermetallics* **7** 315
[15] Meyer B and Fähnle M 1999 *Phys. Rev.* B **59** 6072
[16] Bester G, Meyer B and Fähnle M 1999 *Phys. Rev.* B **60** 14 492
[17] Monkhorst H J and Pack J D 1976 *Phys. Rev.* B **13** 5188
[18] Chadi D J and Cohen M L 1973 *Phys. Rev.* B **8** 5747
[19] Hong T, Watson-Yang T J, Freeman A J, Oguchi T and Xu J 1990 *Phys. Rev.* B **41** 12 462
[20] Rose J H, Ferrante J and Smith J R 1981 *Phys. Rev. Lett.* **47** 675
[21] Villars P and Calvert L D 1986 *Pearson's Handbook of Crystallographic Data for Intermetallic Phases* (Metals Park, OH: American Society for Metals)
[22] Carlsson A E and Meschter P J 1989 *J. Mater. Res.* **4** 1060
[23] Börnsen N, Bester G, Meyer B and Fähnle M 2000 *J. Alloys Compounds* **308** 1
[24] Schultz P A and Davenport J W 1993 *J. Alloys Compounds* **197** 229